

We are IntechOpen, the world's leading publisher of Open Access books Built by scientists, for scientists

6,900

Open access books available

186,000

International authors and editors

200M

Downloads

Our authors are among the

154

Countries delivered to

TOP 1%

most cited scientists

12.2%

Contributors from top 500 universities



WEB OF SCIENCE™

Selection of our books indexed in the Book Citation Index
in Web of Science™ Core Collection (BKCI)

Interested in publishing with us?
Contact book.department@intechopen.com

Numbers displayed above are based on latest data collected.
For more information visit www.intechopen.com



Nondestructive and Contactless Characterization Method for Spatial Mapping of the Thickness and Electrical Properties in Homo-Epitaxially Grown SiC Epilayers Using Infrared Reflectance Spectroscopy

Sadafumi Yoshida, Yasuto Hijikata and
Hiroyuki Yaguchi

Additional information is available at the end of the chapter

<http://dx.doi.org/10.5772/50749>

1. Introduction

Silicon carbide (SiC) is one of the most promising semiconducting materials for the fabrication of high power electronic devices with extremely low loss, owing to its excellent physical properties, such as high breakdown electric field, high saturation electron drift velocity, and high thermal conductivity. Nowadays, some kinds of devices, such as SBDs, JFETs and MOSFETs have been on the market. For the fabrication of SiC devices with high yield rates, *i.e.*, for reducing the scattering of device specification, the production of high-quality, large-diameter epi-wafers with uniform thickness and electrical properties is indispensable. In order to characterize the electrical and thickness uniformity of the epi-wafers during the device process, *i.e.*, to know how the thickness, doping concentration and mobility are distributed over the SiC epi-layers, it is necessary to develop the characterization method that can perform the determinations of thickness and electrical properties simultaneously in a nondestructive and noncontact way.

To characterize the distribution of the electrical properties over SiC wafers and homo-epi-wafers, conductivity mapping is often performed [1]. However, the distribution of carrier concentration and mobility cannot provide from the conductivity mapping, because the conductivity depends both on the distribution of dopant concentration and the crystallinity and/or distribution of crystal defects. In order to characterize the distribution of carrier concentration and mobility over epi-layers, electrical measurement techniques such as Hall ef-

fect measurements and capacitance-voltage ($C-V$) measurements have been widely used. These techniques, however, are disadvantageous as a device fabrication process monitoring tool because they require the formation of electrodes on a sample. By using a mercury probe as an electrode, $C-V$ measurements can be performed without the formation of electrodes on a sample. However, the problems caused by the contamination with mercury contact have been pointed out, recently.

Optical measurement techniques such as Raman scattering spectroscopy [2-5], infrared (IR) spectroscopic ellipsometry [6], optical absorption measurements [7] have been used to estimate the carrier concentration in SiC wafers as a nondestructive and contactless method. IR reflectance measurements have been used to estimate the electrical properties of GaAs [8] and SiC [9]. Macmillan *et al.* [10] reported that the thickness of homo-epitaxially grown SiC wafers can be estimated from the interference oscillations in IR reflectance spectra observed both below and upper frequency ranges of the reststrahlen band ($800-1000\text{cm}^{-1}$ for SiC). Nowadays, the reflectance measurements in near IR spectral range ($1000-4000\text{cm}^{-1}$) is widely used to estimate the thickness of homo-epitaxially grown SiC layers in the SiC device process. As the thickness of epilayers used for power devices are in the range from several to several tens μm , the observation of reflectance spectra in near IR spectral range is suitable to analyze the oscillation of reflectance caused by the interference effects of light in the epilayers.

We have developed the method of obtaining the thickness and electrical properties of semiconductor wafers and epi-wafers, simultaneously, by using IR reflectance spectroscopy [11-15]. In this paper, we will summarize the development of the method, and will discuss the validity of the electrical properties derived from the IR reflectance by comparing with those estimated from Hall effect and $C-V$ measurements. Finally, we will show the results of applying this method to characterize the electrical activation of impurity and crystalline damages in the ion-implanted, and post-implantation-annealed SiC epilayers.

2. Characterization method of the electrical properties in SiC wafers using IR reflectance spectroscopy

2.1. Method of obtaining carrier concentration and mobility from IR reflectance spectroscopy [11,12]

The values of dielectric constants of semiconductors in IR spectral region can be calculated as a function of wavelength or frequency using the dispersion equation. For the analysis of IR reflectance spectra, a number of dielectric function models have been proposed [16-20]. The classical dielectric function (CDF) model [16], which assumes the damping constant of the LO phonon is the same as that of the TO phonon, has been widely used. In the case of wide bandgap semiconductors with an overdamped plasmon system like SiC, the reflectance spectrum is, however, strongly dependent on LO-phonon damping because the plasmon is overdamped and the LO phonon frequency is much higher than the plasma frequency except for heavily doped cases. For these reasons, we have chosen to use the modified classi-

cal dielectric function (MDF) model taking into account the contribution of the TO phonon damping constant and the LO phonon damping constant independently [17]. Considering the contributions from phonons and plasmons, the dielectric constant is given as

$$\varepsilon(\omega) = \varepsilon_{\infty} \left(\frac{\omega_L^2 - \omega^2 - i\Gamma_L \omega}{\omega_T^2 - \omega^2 - i\Gamma_T \omega} - \frac{\omega_p^2}{\omega^2 + i\gamma_p \omega} \right) \quad (1)$$

where ε_{∞} is the high frequency dielectric constant, ω_T and ω_L are the TO- and LO-phonon frequencies, respectively, Γ_T and Γ_L are the TO- and LO-phonon damping constants, respectively, γ_p is the free-carrier damping constant, and ω_p is the plasma frequency of the free carriers, which is given by

$$\omega_p = \sqrt{\frac{N e^2}{m^* \varepsilon_{\infty}}} \quad (2)$$

where N , e , and m^* are the free carrier concentration, electron charge, and effective mass, respectively. The free-carrier damping constant γ_p is the inverse of the scattering time τ and therefore the free-carrier mobility can be derived using the following relation,

$$\mu = \frac{e}{m^* \gamma_p} \quad (3)$$

Assuming that the wafers are uniformed in the depth direction, we used the normal-incidence reflectance of a semi-infinite medium R , which is expressed as

$$R(\omega) = \frac{(n-1)^2 + k^2}{(n+1)^2 + k^2} \quad (4)$$

where n and k are the optical constants, derived from $\varepsilon/\varepsilon_0 = (n-ik)^2$.

The carrier concentration and mobility can be determined by fitting the experimental infrared reflectance spectrum with calculated ones. To fit the spectra, we used the least-squares method based on eqs. (1) and (4), where we adopted ω_p , γ_p , and Γ_L as adjustable parameters.

2.2. Measurements of IR reflectance spectra of SiC wafers and estimation of electrical properties [12]

Single crystal wafers of commercially produced n -type (nitrogen doped) 6H-SiC were used. IR reflectance spectra were measured using two Fourier-transform infrared (FTIR) spectrometers, JASCO FT/IR-VM7 for the far-infrared region (30–600 cm^{-1}) and JASCO FT/IR 670-PLUS for the middle-infrared region (400–2000 cm^{-1}), respectively. For far-infrared reflectance measurements, two light sources (a mercury arc-lamp and nichrome light source),

three beam splitters (4, 12, 25 μm thick Mylar films) and a p-DTGS (pyroelectric deuterated triglycine sulfate) detector were used. For middle-infrared reflectance measurements, a high intensity ceramic light source, a KBr beam splitter, and a TGS detector were employed. Each IR reflectance spectrum was measured with 1 cm^{-1} spectral resolution. The light diameters were 5 mm for far-infrared measurements, and 3 mm for middle-infrared measurements. The measurements were performed for (0001) Si-faces of 6H-SiC wafers at nearly normal incidence. An Al mirror was used as a reflectance reference.

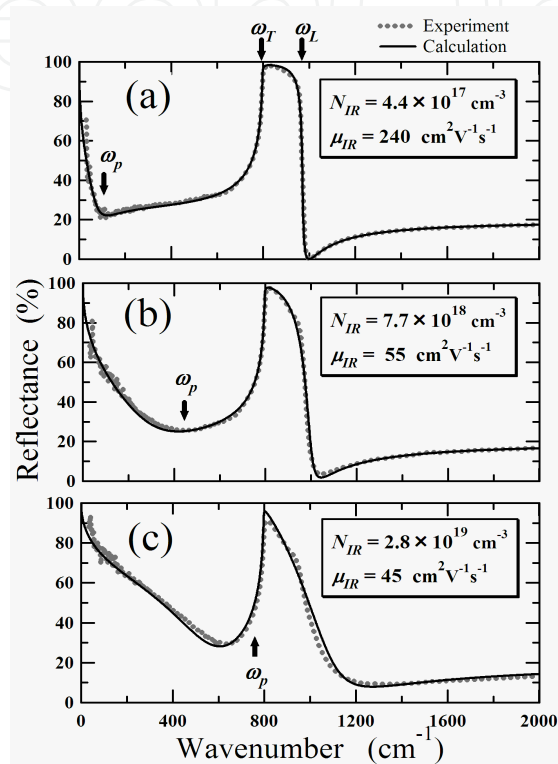


Figure 1. Infrared reflectance spectra measured for 6H-SiC wafers with various carrier concentrations at room temperature (dotted line). The solid lines show the fitted spectra calculated using MDF model. The values of carrier concentration and mobility obtained from fitting to the measured IR spectra are described in the figure [12].

The dotted lines in Figure 1 show the typical infrared reflectance spectra of several 6H-SiC wafers of different carrier concentrations at room temperature. The plasma edges and reststrahlen bands appear in the far-IR and middle-IR regions, respectively. We derived the values of carrier concentration and mobility by the curve fitting of calculated curves to the observed ones. For the curve fitting, we chose ω_p , Γ_L , γ_p as adjustable parameters. For the values of the other parameters, we employed those obtained from Raman scattering measurements, $\epsilon_\infty = 6.52\epsilon_0$, $\omega_T = 797\text{ cm}^{-1}$, $\omega_L = 969.4\text{ cm}^{-1}$, $\Gamma_T = 2\text{ cm}^{-1}$, and $m^* = 0.35m_0$ for 6H-SiC[2]. Since the light is normally incident on the (0001) face of the samples, these parameters are all for the modes vibrating perpendicular to the c-axis.

From the curve fitting analysis, we obtained a good fit for each experimental spectrum, which was obtained by measuring nine samples with carrier concentrations in the range of $4 \times 10^{17} \sim 3 \times 10^{19}\text{ cm}^{-3}$. The solid lines in Figure 1 show examples of the fitted curves obtained by fitting to the typical IR reflectance spectra shown as the dotted line in each figure. The free-

carrier concentration and drift mobility were derived from the best-fit parameters of ω_p and γ_p using eqs.(2) and (3), mentioned above. The values of free-carrier concentration and mobility obtained are also given in each figure.

As shown in Figure 1 (c), there is a slight discrepancy at approximately 900 cm^{-1} between the spectrum observed and that calculated using the MDF model (eq. (1)). This discrepancy increases with increasing carrier concentration in the high 10^{19} cm^{-3} range. For heavily doped SiC crystals, the CDF and MDF models would be inappropriate because the MDF model is derived considering the effects of phonons and plasmons independently. In the case of heavily doped SiC crystals, the plasma frequency is closed to the phonon frequency and the LO phonon and plasmon are strongly coupled. Therefore, though the MDF mode can approximately estimate the electrical properties of heavily doped SiC wafer, it is necessary to use another dielectric function mode that takes into account the effect of LO phonon-plasmon coupled modes [19,20] to obtain more accurate values.

2.3. Comparison with the values derived from Hall effect measurements [12]

For the confirmation of the validity of the values of carrier concentration and mobility derived from IR reflectance spectra, we performed Hall effect measurements for the same samples used for IR reflectance measurements and compared between the values obtained from the optical and electrical methods. The 6H-SiC wafers with a wide variety of carrier concentrations ranging from 3.4×10^{17} to $2.4 \times 10^{19}\text{ cm}^{-3}$ were used.

We cut the SiC wafers to a size of $5 \times 5\text{ mm}^2$ for the Hall effect measurements using van der Pauw method. After chemical cleaning, ohmic contacts were fabricated at the corners of each sample by the evaporation of nickel and subsequent heat treatment at 1000°C for 10 min. IR reflectance measurement and Hall measurement were carried out at room temperature.

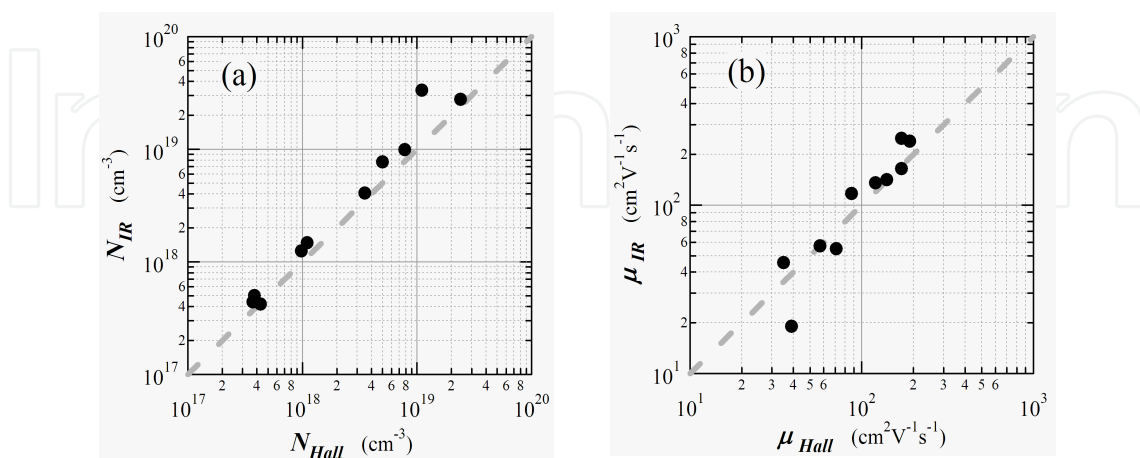


Figure 2. Comparison of (a) carrier concentration and (b) mobility values, N_{IR} , μ_{IR} obtained from IR reflectance spectroscopy measurements with those from Hall effect measurements, N_{Hall} , μ_{Hall} . The broken lines represent the case of complete agreement with each other [12].

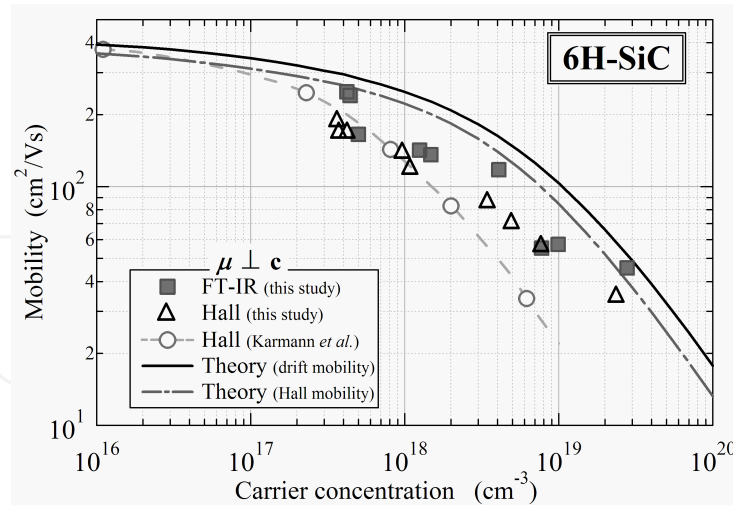


Figure 3. The variations in drift mobility evaluated from IR reflectance spectroscopy, and Hall mobility measurements plotted against carrier concentration. The reported values of Hall mobility [23] and those calculated theoretically ($N_A/N_D=0$) following reference [24] are also shown for comparison [12].

In Figure 2 (a) and (b), the carrier concentrations and mobilities estimated from the IR reflectance spectra are plotted against those obtained from the Hall effect measurements. As the reported Hall scattering factor r_H is approximately unity at room temperature for 6H-SiC [21,22], we assumed r_H is equal to unity for the calculation. Good agreement was obtained between the electrical characteristics obtained from IR reflectance measurements and those from Hall effect measurements.

The LO phonon damping constant Γ_L which is one of the adjustable parameters, varies linearly with carrier concentration. This tendency is in good agreement with the results obtained by Raman scattering spectroscopy [17] in which, as was explained, the interactions between ionized impurity and LO phonon, and free carrier and LO phonon increase with increasing doping concentration.

In Figure 3, the drift mobility and Hall mobility of the 6H-SiC wafers are plotted against the determined free carrier concentration, and against those reported by Karmann *et al* [23]. The Hall mobilities obtained in the present study are a little higher than those determined by Karmann *et al.* in a high-carrier-concentration region. We calculated the drift and Hall mobility at room temperature as functions of dopant concentration following references [24-26], assuming that the compensation ratio $N_A/N_D=0$, and considered five carrier scattering mechanisms (acoustic phonon deformation potential scattering, polar optical phonon scattering, intervalley phonon deformation potential scattering, neutral impurity scattering, and ionized impurity scattering) as in reference [29]. The values of the mobility obtained in this work are lower than those obtained from the theoretical calculations. This result suggests that the compensation ratio is not 0 but approximately 0.2 in this study and a little higher in the case of Karmann *et al.*

Through comparison, we have ascertained that the electrical characteristics of SiC wafers can be estimated by IR reflectance spectroscopy with high credibility.

2.4. Spatial mapping of the electrical properties over SiC wafers [11,12]

To demonstrate the capability of the method proposed, we performed the spatial mapping of the distribution of the carrier concentration and mobility of a commercially produced 2 inch 6H-SiC wafer. For the spatial mapping, we employed a micro FTIR (JASCO Irtron IRT-30 infrared microscope), which was equipped with a mercury cadmium telluride (MCT) detector. The diameter of the beam was 0.1 mm and the interval between measured points was 5 mm (a total of 120 measurement points). We performed the measurements in the spectral range of 560–2000 cm^{-1} with a spectral resolution of 4cm^{-1} .

Figure 4 shows an example of the spatial distribution of the free-carrier concentration and mobility of a commercially produced 2-inch 6H-SiC wafer obtained using this technique. This measurement technique needs no prior surface treatment, because the native oxide layer thickness and surface roughness are not more than 3 nm and their influence on the reflectance spectra is negligible in IR region. The uniformity of free-carrier concentration and mobility throughout this wafer except for 5 mm from the edge were estimated to be approximately $\pm 9\%$ and $\pm 15\%$, respectively. The free-carrier concentration mapping shows that the free-carrier concentration in the central region is greater than that in the edge region. On the other hand, the mobility mapping shows the negative correlation of the mobility distribution with that of carrier concentration. When conductivity mapping is used as the method for the mapping of electrical properties of the wafer, it leads to the misleading conclusion that the electrical uniformity over the wafers is approximately $\pm 5\%$ and the wafer is almost uniform, because the conductivity is determined as the product of carrier concentration and mobility. Therefore, the proposed IR reflectance spectroscopic method is more appropriate for the characterization of the distribution of the electrical properties of SiC wafers.

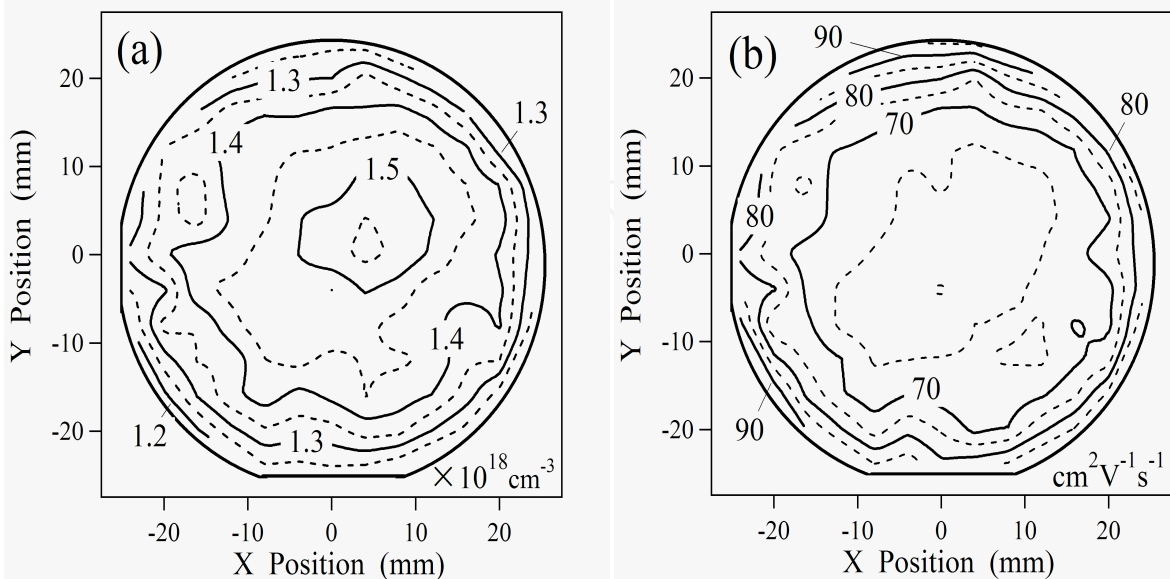


Figure 4. Spatial mapping of (a) carrier concentration and (b) mobility in a commercially produced 2 inch 6H-SiC wafer [12].

3. Characterization method of the electrical properties and thickness of epilayers using IR reflectance spectroscopy

3.1. Method of obtaining the carrier concentration, mobility, and thickness of epilayers, simultaneously [13]

In this section, we propose the method for the simultaneous determination of the electrical properties, *i.e.*, free carrier concentration and mobility, and the thickness of epilayers as well as bulk layer by IR reflectance measurements. First, we will explain the procedure of obtaining carrier concentration, mobility and thickness of the epilayers on SiC wafers. Then, we will compare the electrical properties derived from the IR reflectance analyses with those from Hall effect measurements for *n*-type epilayers grown on *p*-type substrates, and with those from *C-V* measurements in the case of *n*-type epilayers on *n*-type substrates. Finally we will discuss the validity of the obtained values from the proposed method.

The carrier concentration and mobility of epilayers and substrates, as well as the thickness of the epilayers can be determined simultaneously by fitting the calculated reflectance spectra to measured ones. The reflectance *R* from an air/ epilayer/substrate structure at normal incidence is given by

$$R = \left| \frac{r_1 + r_2 e^{-2i\delta}}{1 + r_1 r_2 e^{-2i\delta}} \right|^2, \quad \text{where} \quad \delta = \frac{2\pi n d}{\lambda} \quad (5)$$

where r_1 and r_2 are the Fresnel reflection coefficients at the air/epilayer and the epilayer/substrate interface, respectively, and δ is the phase shift of light in the epilayer, n and d are the refractive index and the thickness of epilayer, respectively, and λ is wavelength. The optical constants of SiC in IR spectral range are derived from the dielectric constants as a function of the frequency of the incident light, given by eq.(1) both for substrate and epilayer. As in the case of SiC bare wafers written in Section 2, we fitted the calculated spectrum to the measured one by adjusting the values of ω_p , γ_p , Γ_T and Γ_L of the epilayer and those of the substrate, and the epilayer thickness d . From these values, we can obtain the carrier concentration N and mobility μ of the epilayer and substrate using eqs. (3) and (4). In the calculation, we adopted the values $\epsilon_\infty=6.56$, $\omega_T=798\text{cm}^{-1}$, $\omega_L=970\text{cm}^{-1}$, and $m_{\text{MG}}^*=0.58m_0$, $m_{\text{MK}}^*=0.31m_0$, obtained from the Raman scattering measurements of 4H-SiC [2] and optical detection of cyclotron resonance (ODCR) [27]. Considering that the free carriers distribute themselves in proportion to the square root of each effective mass, the averaged effective mass, $m^*=(m_{\text{MK}}^*m_{\text{MG}}^*)^{1/2}$, and $m^*=(1/m_{\text{MK}}^{*1/2}+1/m_{\text{MG}}^{*1/2})/(1/m_{\text{MK}}^{*3/2}+1/m_{\text{MG}}^{*3/2})$ were used for the calculation of the carrier concentration and mobility, respectively.

3.2. Measurements of IR reflectance spectra and derivation of electrical properties and thickness of SiC epi-wafers [13]

Samples used in this study were nitrogen doped *n*-type 4H-SiC epilayers grown on *n*- and *p*-type 4H-SiC substrates supplied from National Institute of Advanced Industrial Science and Technology (AIST). The epilayers were grown on 4H-SiC (0001) Si face 8 off substrates by chemical vapor deposition (CVD). The details of the epilayer growth have been described elsewhere [28]. In the case of the *n*-type epilayers on *p*-type substrates, the carrier concentration of the epilayers was in the range between 3×10^{17} and $2 \times 10^{18} \text{ cm}^{-3}$, and that of the substrates was typically $4 \times 10^{16} \text{ cm}^{-3}$. On the other hand, in the case of the *n*-type epilayers on *n*-type substrates, the net doping concentration ($N_D - N_A$) of the epilayers was in the range between 1×10^{17} and $8 \times 10^{17} \text{ cm}^{-3}$, and that of the substrates was typically $5 \times 10^{18} \text{ cm}^{-3}$. The thickness of the epilayers were 6~7 μm , measured by scanning electron microscope (SEM) observation of the cleaved facet of the samples. The IR reflectance spectra in the frequency range of 80–2000 cm^{-1} were measured at room temperature using same spectrometers mentioned in Section 2.2. Hall effect measurements were performed at room temperature using van der Pauw method for *n*-type epilayers on *p*-type substrates. Ohmic contacts were fabricated on the epilayer surfaces by the electron beam evaporation of Ni and subsequent annealing at 900°C for 30min in N_2 atmosphere. *C-V* measurements were performed at room temperature using a mercury probe as a Schottky contact.

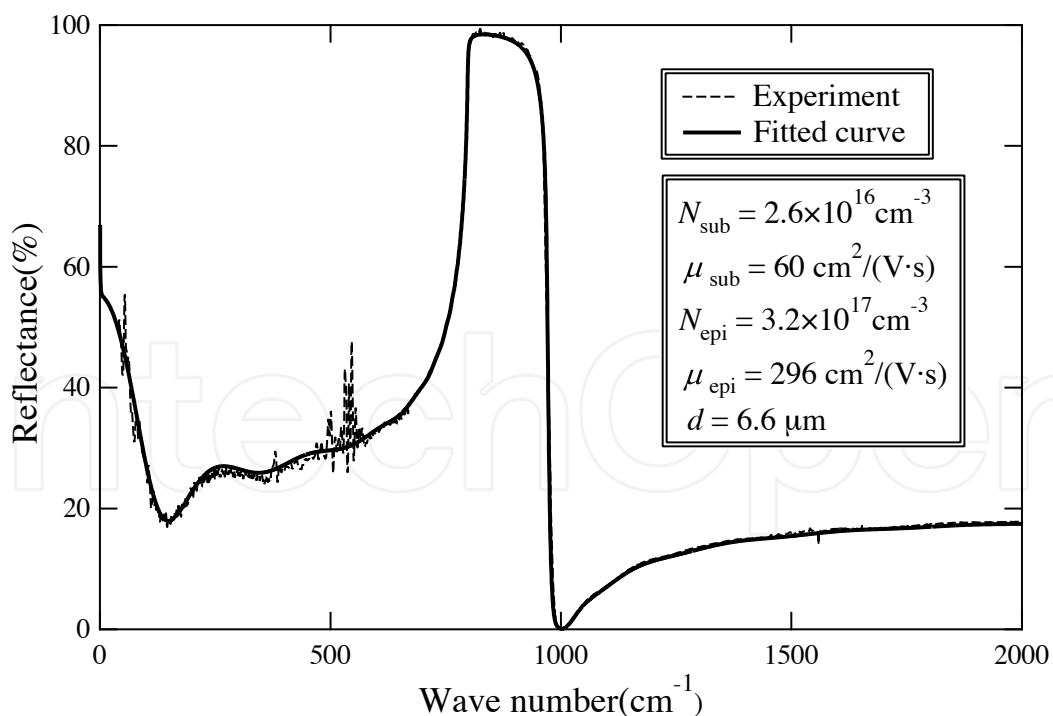


Figure 5. IR reflectance spectrum of an *n*-type epilayer on a *p*-type substrate at room temperature denoted by dashed line. The solid line shows the fitted curve calculated using the MDF model. The values estimated from this fitting are listed in the figure [13].

At first, we estimated the carrier concentration and mobility of n -type epilayers on p -type substrates from the reflectance measurements, and compared with these values obtained from Hall effect measurements. Figure 5 shows typical IR reflectance spectra measured for the n -type epilayers on p -type substrates. The solid line denotes the calculated values fitted to the experimental one shown as the dashed line. The values $N_{\text{epi}} = 3.2 \times 10^{17} \text{ cm}^{-3}$, $\mu_{\text{epi}} = 296 \text{ cm}^2/(\text{V s})$, and $d = 6.60 \text{ }\mu\text{m}$ were obtained by a curve fitting analysis. These values are listed in the figure. In the case of p -type substrate whose carrier concentration is low in general, the reflectance spectrum is almost independent of the electrical properties of the substrate, thus, it is difficult to estimate the carrier concentration and mobility of the substrate. Therefore, we used the values for the p -type substrate without epilayer obtained from the Hall effect measurements. The thickness of the epilayers obtained from the IR reflectance measurements and those measured from the SEM observation coincide with each other within $\pm 1\%$.

The carrier concentrations and mobilities obtained from the IR reflectance measurements are plotted with respect to those obtained from Hall effect measurements in Figures 6 (a) and (b), respectively. Since the Hall scattering factor r_{H} is reported to be approximately unity at room temperature for 4H-SiC [27,29] as in the case of 6H-SiC, we directly compared the drift mobilities estimated from the IR reflectance measurements and those of the Hall mobilities obtained from the Hall effect measurements. The error bars shown in the figures represent the accuracy of the fitting analysis, and the accuracy is about $\pm 4\%$ for both the carrier concentration and the mobility, whereas the accuracy of the values derived from Hall effect measurements is about $\pm 10\%$. As can be seen from these figures, the electrical properties obtained from the reflectance spectra are in good agreement with those obtained from the Hall effect measurements. These results suggest that the proposed method is valid for obtaining the values of carrier concentration and mobility of the epilayers. However, careful observation confirms that the values of carrier concentration and mobility derived from the infrared reflectance measurements are slightly lower than those obtained from the Hall effect measurements. The difference can be explained by the consideration that the part of free carriers trapped in defects or bounded by dopants cannot follow in the THz frequency range used for the reflectance measurements, unlike in Hall effect measurements, where a direct current is supplied.

Next, we estimated the values of carrier concentration and mobility for n -type epilayers on n -type substrates from the IR reflectance spectra measured. Figure 7 shows a typical IR reflectance spectrum observed and its fitted curve. The values $N_{\text{epi}} = 1.3 \times 10^{17} \text{ cm}^{-3}$, $\mu_{\text{epi}} = 403 \text{ cm}^2/(\text{V s})$ and $d = 4.45 \text{ }\mu\text{m}$; and $N_{\text{sub}} = 7.1 \times 10^{18} \text{ cm}^{-3}$, $\mu_{\text{sub}} = 53 \text{ cm}^2/(\text{V s})$ were obtained by curve fitting analysis as the parameters of the epilayer and substrate, respectively. The accuracy of the carrier concentration and mobility of epilayers derived from the fitting of the IR reflectance spectrum is about $\pm 10\%$. In Figure 8, the free carrier concentration estimated from the IR reflectance spectra is plotted with respect to the net doping concentrations $N_{\text{D}} - N_{\text{A}}$ derived from C - V measurements. We calculated the free carrier concentrations n from the net doping concentrations using

$$n(T) + N_A = \frac{N(h)}{1 + \{gn(T)/N_C\} \exp[\Delta E(h)/k_B T]} + \frac{N(k)}{1 + \{gn(T)/N_C\} \exp[\Delta E(k)/k_B T]} \quad (6)$$

$$N_C = 2M_C \left(\frac{m^*_{d.s.} k_B T}{2\pi \hbar^2} \right)^{3/2} \quad (7)$$

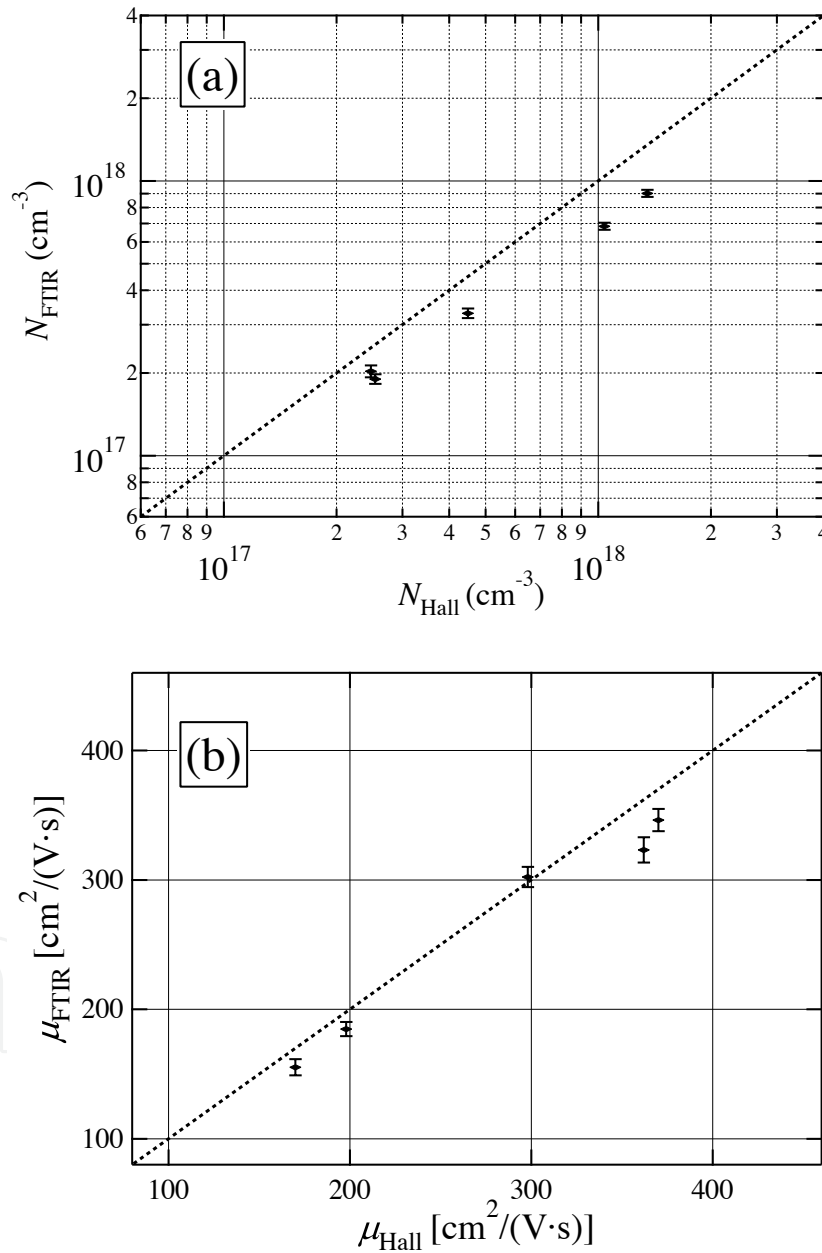


Figure 6. Values of (a) carrier concentration and (b) mobility estimated from IR reflectance measurements and Hall effect measurements. The dotted line in the figures corresponds to the case of complete agreement with each other [13].

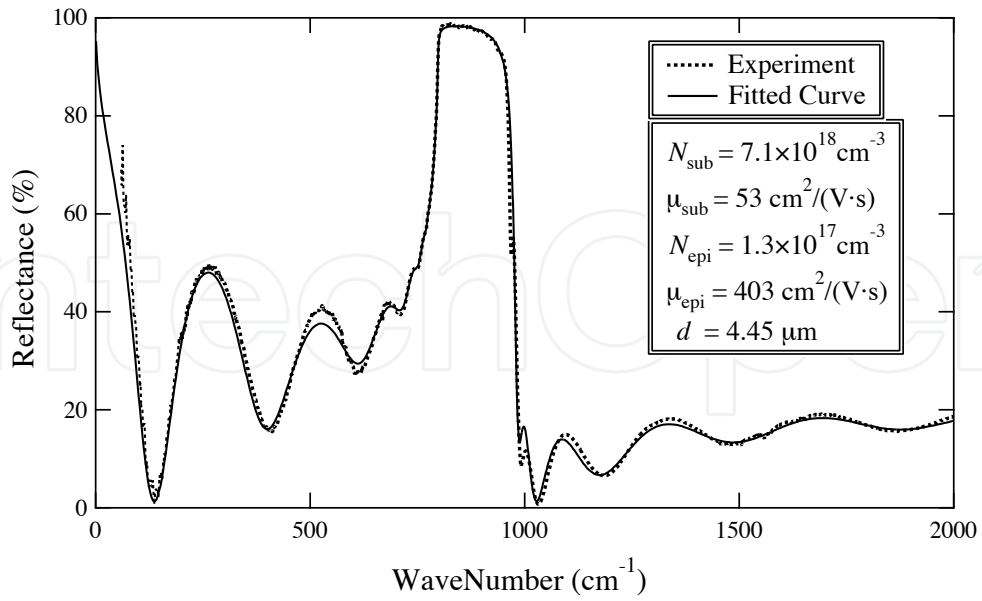


Figure 7. IR reflectance spectrum of an *n*-type epilayer on an *n*-type substrate denoted by dashed line. The solid line shows the fitted curve calculated using the MDF model. The values estimated from this fitting analysis are listed in the figure [13].

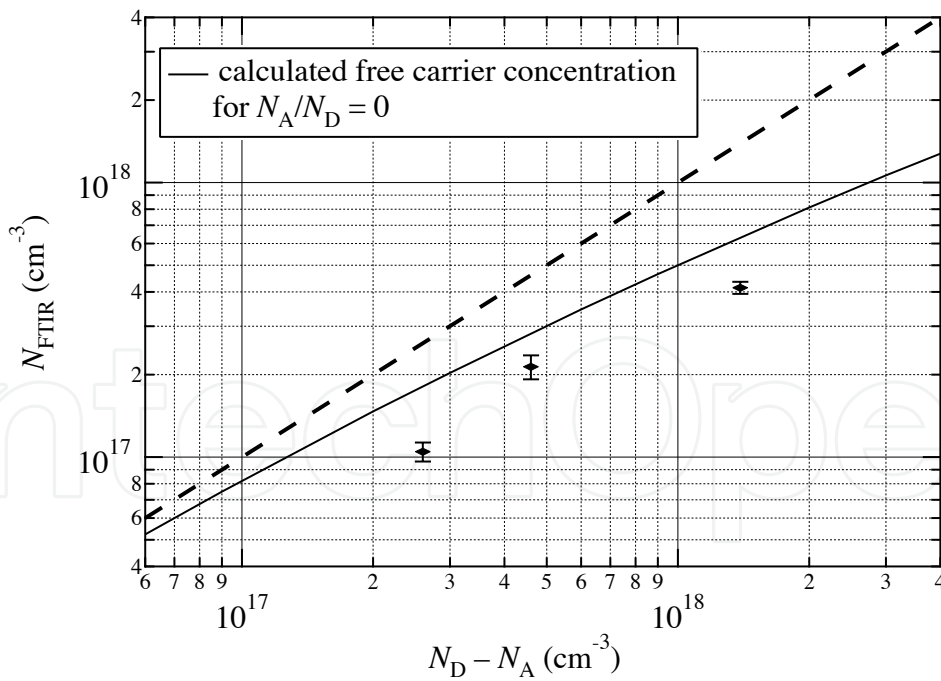


Figure 8. Values of the carrier concentration estimated from the IR reflectance for *n*-type epilayers on *n*-type substrates as a function of dopant concentration obtained from C-V measurements for each sample. The solid line represents the theoretical carrier concentration for T=300K assuming zero doping concentration ($N_A=0$) using eq. (6). The dashed line represents $N_{FTIR}=N_D-N_A$ [13].

where k_B is the Boltzmann constant, T is the temperature, N_A is the concentration of acceptors, and $N(h)$ and $N(k)$ are the concentrations of the nitrogens occupied at hexagonal and cubic lattice sites, respectively. Since the number of hexagonal sites is equal to those of cubic sites for 4H-SiC, the donor concentration N_D is given by $N(h) + N(k)$. The values of $\Delta E(h)$ and $\Delta E(k)$ are the ionization energies of the nitrogen donor at hexagonal and cubic lattice sites, respectively, and $g = 2$ is the spin degeneracy factor. Equation (7) gives the effective density of states, where $M_c = 3$ is the number of equivalent conduction band minima, and $m_{d.s.}^*$ is the density-of-states effective mass. The values of $\Delta E(h)$ and $\Delta E(k)$ were set as 50 meV and 100 meV, respectively, referring to the reported experimental data [30,31]. The values of $m_{MT}^* = 0.58m_0$, $m_{MK}^* = 0.31m_0$, $m_{ML}^* = 0.33m_0$ derived from ODCR measurements [27] were adopted. The solid line in Figure 8 shows the free carrier concentrations calculated as a function of the net doping concentration, where we assumed that $N_A/N_D = 0$ or $N_D/(N_A + N_D) = 1$, because the epilayers we measured are hardly compensated [32]. The values obtained from the IR reflectance spectra are slightly lower than the calculated values, as in the case for the samples of n -type epilayers on p -type substrates. The value of drift mobility calculated in consideration of five carrier scattering mechanisms [24] is $340 \text{ cm}^2/(\text{Vs})$, in the case of $N_A/N_D = 0$ and $N_D - N_A = 2.7 \times 10^{17} \text{ cm}^{-3}$, which is almost the same as the value obtained from the IR reflectance spectrum, *i.e.*, $403 \text{ cm}^2/(\text{Vs})$. This result also indicates that the compensation of the sample is low.

3.3. Extension of the carrier concentration range down to 10^{16} cm^{-3} order using Terahertz frequency range [14]

We have shown that the carrier concentration and mobility of substrate and epilayers as well as the thickness of epilayer are obtained simultaneously from IR reflectance spectra in the frequency range of $80\text{--}2000 \text{ cm}^{-1}$, and confirmed that the values of the carrier concentration, mobility and epilayer thickness estimated from IR reflectance spectroscopy are valid. However, it was difficult to estimate the electrical properties of homo-epilayers with carrier concentrations less than $1 \times 10^{17} \text{ cm}^{-3}$ without IR reflectance spectra less than 80 cm^{-1} . Figure 9 is the variation of plasma frequency with carrier concentration calculated from eq.(2) for 4H-SiC. The figure indicates the plasma frequencies are smaller than 100 cm^{-1} for the carrier concentration less than 10^{17} cm^{-3} . Figure 10 shows the variations of the reflectance spectrum of epilayers with the decrease of carrier concentrations from 3×10^{18} to $3 \times 10^{16} \text{ cm}^{-3}$. The magnified features of the calculated reflectance spectra for $1 \times 10^{17} \text{ cm}^{-3}$, 5×10^{16} , and $1\text{--}5 \times 10^{15} \text{ cm}^{-3}$ in Terahertz frequency range are shown in Figure 11. These figures suggest that it is necessary to measure a spectrum down to around 20 cm^{-1} for extending the carrier concentration down to the order of 10^{16} cm^{-3} .

From these considerations, we extended the spectral range of the reflectance measurements down to 20 cm^{-1} (0.6 THz) by using terahertz reflectance spectroscopy to be able to apply the method for epilayers with the carrier concentrations in the range of 10^{16} cm^{-3} . Also we have compared the free carrier concentrations estimated from reflectance measurements with the net doping concentrations obtained from $C\text{--}V$ measurements to discuss the validity of this characterization method.

Samples used in this study were nitrogen doped n -type 4H-SiC epilayers grown on n -type 4H-SiC substrates by chemical vapor deposition (CVD) [28]. The net doping concentration ($N_D - N_A$) of the epilayers was in the range between 5×10^{16} and $1 \times 10^{18} \text{ cm}^{-3}$, and that of the substrates was typically $5 \times 10^{18} \text{ cm}^{-3}$. The thickness of the epilayers was 6–7 μm , measured by SEM observation. C - V measurements were performed using gold electrodes evaporated on the samples as Schottky contacts. The reflectance spectra were measured at room temperature for the spectral region of 20–100 cm^{-1} , 80–600 cm^{-1} and 540–2000 cm^{-1} using terahertz time-domain spectroscopy (THz-TDS) (*Aispec*: pulse IRS 1000/2000), FTIR spectrometers (*JASCO*: IR-VM7) and (*JASCO*: Irtron IRT-30), respectively.

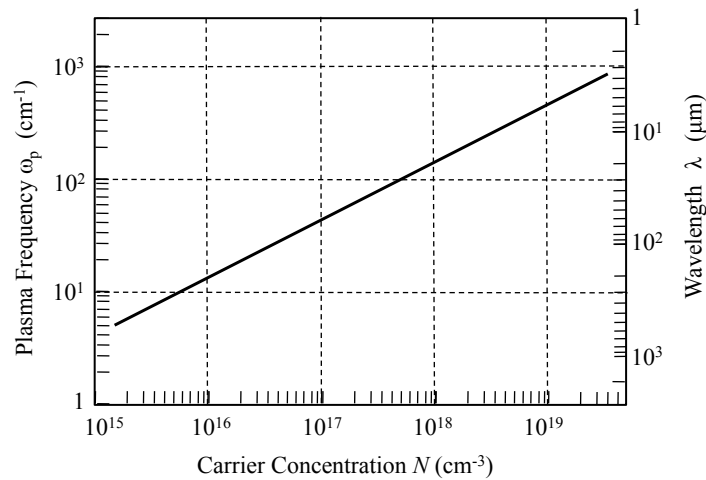


Figure 9. Variation of plasma frequency ω_p with carrier concentration N .

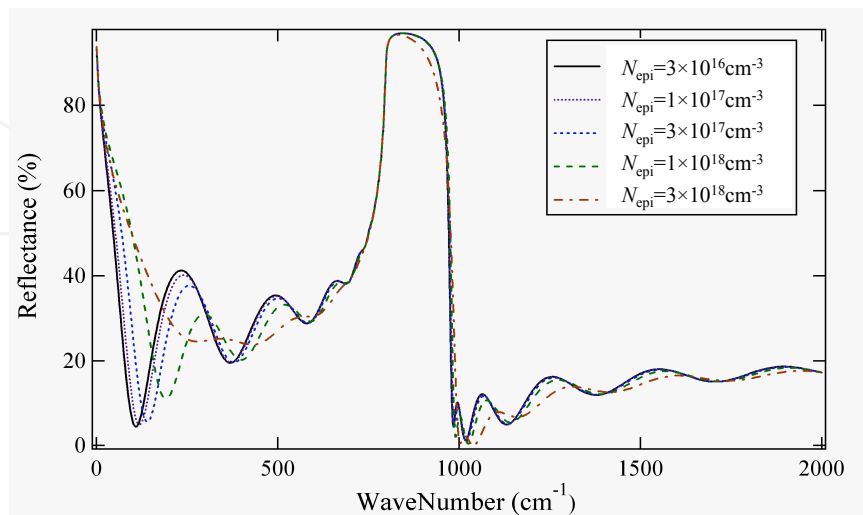


Figure 10. Calculated reflectance spectra of the SiC epilayers (3 μm thick) with various carrier concentrations on a SiC wafer ($N_{\text{sub}} = 5.5 \times 10^{18}$, $\mu_{\text{sub}} = 50 \text{ cm}^2/\text{Vs}$).

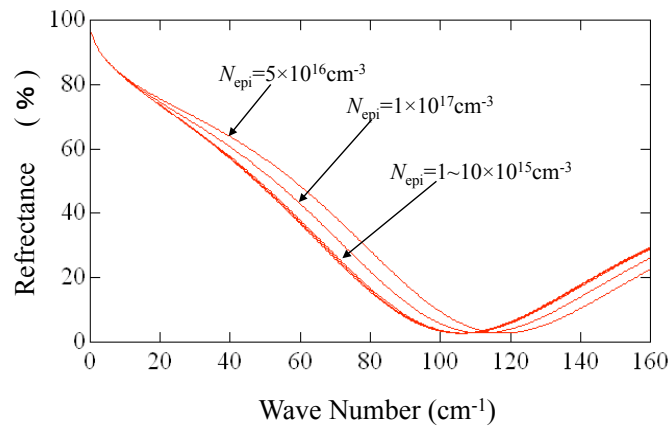


Figure 11. Calculated reflectance spectra of the SiC epilayers (5 μm thick) with low carrier concentrations on a SiC wafer ($N_{\text{sub}}=4\times 10^{18}\text{cm}^{-3}$, $\mu_{\text{sub}}=50\text{cm}^2/\text{Vs}$).

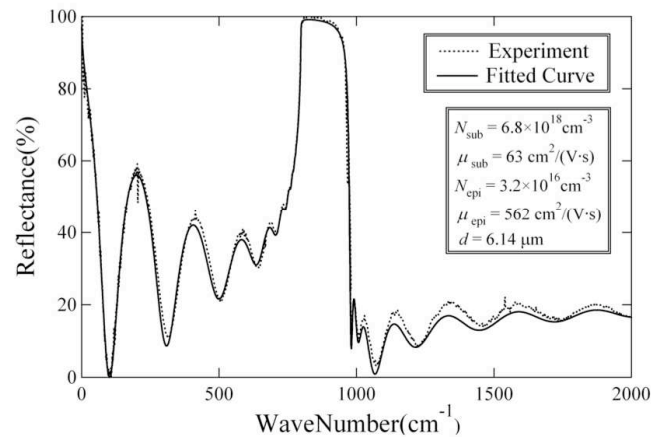


Figure 12. Measured and calculated reflectance spectra of an n -type epilayer on an n -type substrate at room temperature. The values estimated from this fitting analysis are listed in the figure [14].

We have estimated the values of carrier concentration and mobility for the samples of n -type epilayers on n -type substrates from the IR reflectance spectra measured. Figure 12 shows the measured and calculated reflectance spectra of the epilayer with a net doping concentration around $5\times 10^{16}\text{cm}^{-3}$ at room temperature. As shown in the figure, reflectance spectrum measured by THz reflectance spectroscopy are well connected with that measured by IR reflectance spectroscopy at around 100cm^{-1} , and we obtained a good fit between the measured and the calculated spectrum. From the values of fitting parameters, the values $N_{\text{epi}} = 3.2\times 10^{16}\text{cm}^{-3}$, $\mu_{\text{epi}} = 562\text{cm}^2/(\text{V}\cdot\text{s})$ and $d = 6.14\mu\text{m}$, and $N_{\text{sub}} = 6.8\times 10^{18}\text{cm}^{-3}$, $\mu_{\text{sub}} = 63\text{cm}^2/(\text{V}\cdot\text{s})$ were obtained.

In Figure 13, the free carrier concentrations estimated from the IR reflectance spectra are plotted against the net doping concentrations $N_D - N_A$ derived from $C-V$ measurements. We calculated the free carrier concentrations n from the net doping concentrations using eq.(6). The solid line in the figure shows the free carrier concentrations calculated as a function of net doping concentration. We assumed that $N_A / N_D = 0$ or $N_D / (N_A + N_D) = 1$, because the epilayers we measured are hardly carrier-compensated [32]. The values obtained from the

reflectance spectra are in fairly good agreement with solid line, suggesting that the values of the carrier concentrations estimated from IR reflectance spectra have a sufficient validity. However, a careful look confirms that the values of carrier concentration derived from the reflectance measurements are slightly lower than those estimated from the electrical measurements as in the case of carrier concentrations higher than 10^{17}cm^{-3} . The same tendency was observed in the comparisons with the Hall effect measurements for the samples of *n*-type epilayers on *p*-type substrates as shown in Figure 8. This tendency is considered to be partly because of the adoption of inappropriate effective mass values for the calculation of reflectance spectra. It is also considered as a cause that the part of free carriers trapped in the defects or bounded by dopants cannot follow in the THz frequency range used for the reflectance measurements, as mentioned above.

4. Characterization of electrical properties and residual crystalline damage in ion-implanted and post-implantation-annealed 4H-SiC epilayers using IR reflectance spectroscopy

4.1. Method of obtaining the electrical properties and crystalline damage in ion-implanted SiC epilayers [15]

Ion implantation is an indispensable process for selective area doping into crystalline silicon carbide (SiC), because the doping of impurities by thermal diffusion is hard to apply for SiC device process due to very small diffusion constant of impurities in SiC. After the ion implantation, annealing at high temperatures is necessary for activating the dopants electrically as well as recovering the crystallinity of SiC damaged by ion implantation. Hall effect measurements, secondary ion mass spectroscopy (SIMS) and transmission electron microscopy (TEM) have been widely used to characterize the electrical properties, depth profile of the impurities and crystalline damage of implanted layers, respectively. These techniques are, however, inappropriate to use as device process monitoring tools because Hall effect measurement requires the formation of electric contacts, and SIMS and TEM observations result in the destruction of the samples. Recently, the short period and high temperature annealing is used in SiC device process [35]. To make clear the effect of short period high-temperature annealing, we investigated the annealing period dependence at the annealing temperature of 1700°C .

Recently, it has been reported that the crystalline damage induced by ion implantation affects the infrared (IR) reflectance spectra around the reststrahlen region ($\sim 800\text{--}1000\text{ cm}^{-1}$) [33,34], and the difference of carrier concentration between epitaxial layer and substrate induces the interference oscillation in the near IR region ($1000\text{--}4500\text{ cm}^{-1}$). In this study, we performed the IR reflectance measurements in the spectral range between $600\text{ and }8000\text{ cm}^{-1}$ for high-dose phosphorus ion implanted and post-implantation-annealed 4H-SiC wafers to characterize both the electrical properties and crystalline damage of the implanted layers without destruction and contactless.

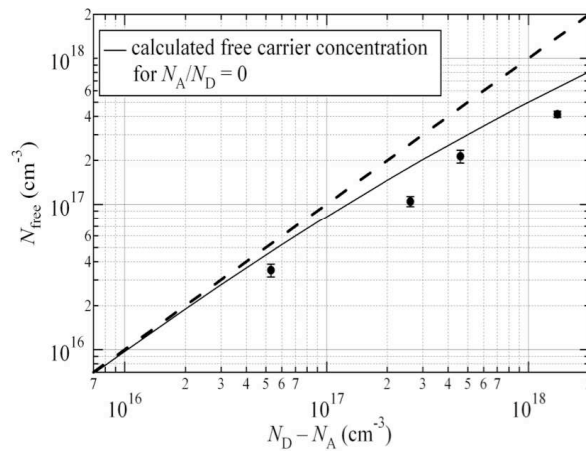


Figure 13. The carrier concentration estimated from the reflectance spectra for an *n*-type epilayer on an *n*-type substrate as a function of doping concentration obtained from *C*-*V* measurements for each sample. The solid line represents the theoretical carrier concentration for $T=300\text{K}$ assuming zero doping concentration ($N_A=0$) using eq. (6). The dotted line represents $N_{\text{FTIR}}=N_D-N_A$ as a guide to the eye [14].

4.2. High-dose phosphorus ion implantation, post-implantation annealing and IR reflectance measurements [15]

The samples used in this study were 4H-SiC (0001) substrates with *p*-type $\sim 5 \mu\text{m}$ thick commercially produced epitaxial layers. The multi-energy implantations of phosphorus ions at 500°C were carried out through the 10 nm thick oxide film in six steps (40–250 keV) in order to form a box-shaped profile with a thickness of $0.3 \mu\text{m}$. The total implanted dose was $7 \times 10^{15} \text{ cm}^{-2}$. After removing the oxide film by HF, the post implantation annealing was conducted in Ar atmosphere. To investigate the annealing temperature dependence of crystalline recovery and electrical properties in the implanted layers, the samples were annealed for 30 min at different temperatures of 1200°C , 1300°C , and 1400°C . In addition, to apply the IR reflectance analysis to the short-period high-temperature annealing process, we also carried out the post implantation annealing at 1700°C for various periods between 0.5 and 10 min. IR reflectance measurements were carried out at room temperature on nearly normal incidence using a micro FT-IR spectrometer (light beam diameter was 0.1 mm). The spectral resolution and range were 4 cm^{-1} and $600\text{--}8000 \text{ cm}^{-1}$, respectively.

4.3. Analysis of carrier concentration, mobility and crystalline damage from IR reflectance spectra [15]

Figure 14 shows the annealing temperature dependence of IR reflectance spectrum. For as-implanted samples, the reflectivity maximum and the shape in the reststrahlen band decreases and becomes blunt, respectively, as compared to those of unimplanted samples. After the high temperature annealing, the reflectivity maximum in the reststrahlen band recovers to that of unimplanted samples. This is resulted from the crystalline recovery in implanted layer. In the spectral range above $\sim 2000 \text{ cm}^{-1}$, the evident interference oscillation is observed. It indicates that the implanted dopants are activated and the refractive index of an

implanted layer is changed by the change of carrier concentration. We can see the tendencies that the reflectance around 1000 cm^{-1} becomes larger with increasing the annealing temperature. We analyzed the observed spectra to evaluate the damage of the ion implantation layers assuming that the implanted layers are composed of two phases, recrystallized SiC phase and defective SiC phase. We have derived the effective dielectric constants ϵ_{eff} of implanted layers using an effective medium approximation (EMA) [33],

$$0 = (1 - f) \frac{\epsilon_c - \epsilon_{eff}}{\epsilon_c + 2\epsilon_{eff}} + f \frac{\epsilon_d - \epsilon_{eff}}{\epsilon_d + 2\epsilon_{eff}} \quad (8)$$

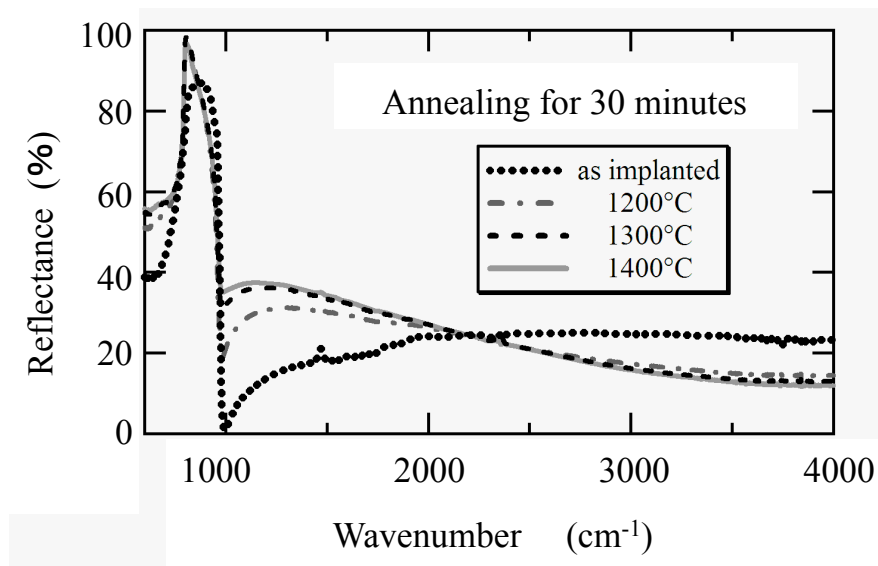


Figure 14. The IR reflectance spectra obtained from the 4H-SiC wafers high-dose implanted and post implantation annealed for 30 minutes [15].

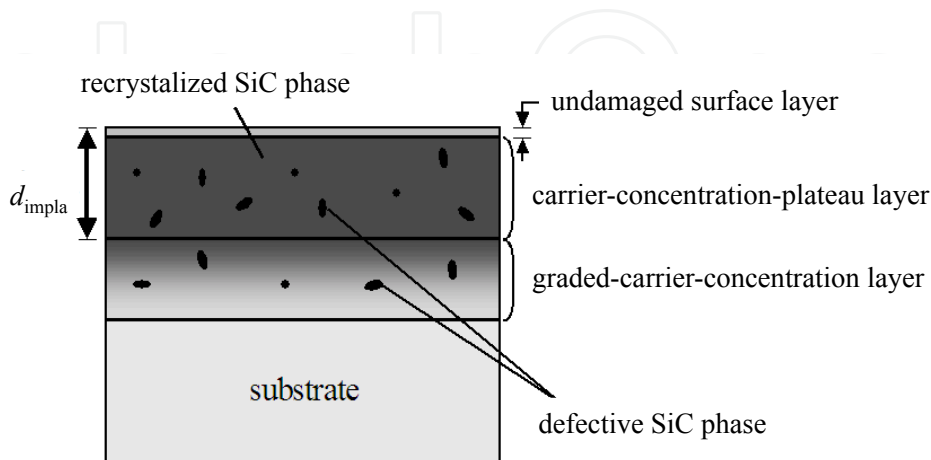


Figure 15. The structural model of the ion implanted SiC wafers used in the calculation of reflectance spectra [15].

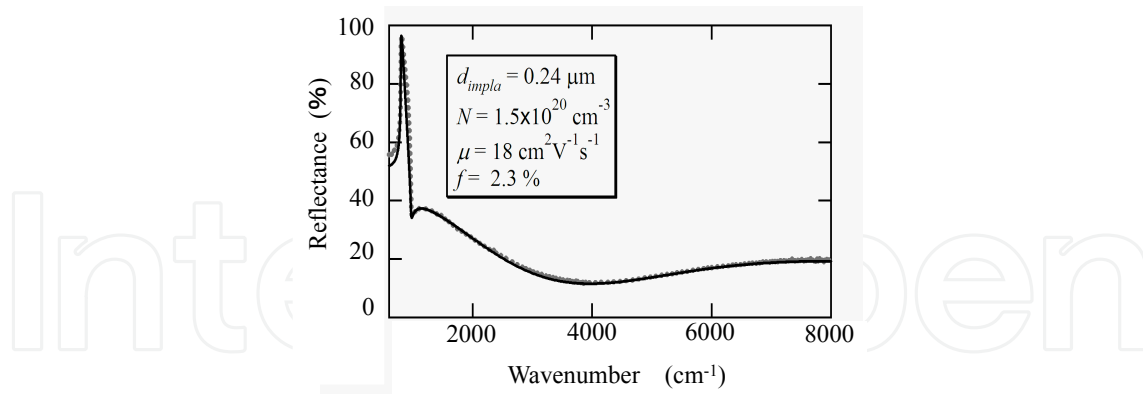


Figure 16. Observed (dotted line) and fitted IR reflectance spectra (solid line) for the samples annealed at 1400°C for 30 min. The best fit parameters are described in the figure [15].

where ϵ_c and ϵ_d are the dielectric constants of re-crystallized and damaged phases, respectively, and f is the volume fraction of damaged phase. We assumed that the frequency dependence of both the dielectric constants of re-crystallized phase and defective phase follows the MDF model given by eq.(1). Referring to the result of TEM observations, we employed the structural model that the ion implanted layer is composed of 3 layers: an undamaged surface layer, a carrier-concentration-plateau layer, and a graded-carrier-concentration layer as shown in Figure 15. Furthermore, we assumed that the volume fraction of defective phase in a graded-carrier-concentration layer is same as that in a carrier-concentration-plateau layer. For a graded-carrier-concentration layer, we used the multi-layer structure approximation assuming that the free carrier concentration decreases exponentially with depth and the mobility changes in inverse proportion to carrier concentration.

4.4. Annealing temperature dependences of electrical activity and re-crystallization [15]

As an example of curve fitting analysis, the spectrum of the sample annealed at 1400°C for 30 min and the fitted curve are shown in Figure 16. We obtained a good fit in the whole spectral region measured. The best-fit parameters derived are also described in the figure. Figure 17 (a) shows the annealing temperature dependence of the volume fraction of the defective phase. By post implantation annealing, the volume fraction of defective SiC drastically decreases from 92 % (as implanted) to 2.9 % (1200°C annealed), and decreases a little with increasing of annealing temperature up to 1400°C. Figure 17 (b) shows the annealing temperature dependence of the carrier concentration (open circle) and the mobility (open triangle) in the re-crystallized phase. For comparison, the electrical properties derived from Hall effect measurements [35] are also plotted in the figure (filled symbols). We can see a good agreement in the electrical characteristics between IR reflectance spectroscopy and Hall effect measurements. The free carrier concentrations are almost constant in the temperature range studied, as in the case of the volume fraction of defective phase. In contrast, the carrier mobility becomes large with increasing the annealing temperature. These results show that the post implantation annealing at a temperature as low as 1200°C reduces the volume fraction of defective SiC drastically and put the impurities in substitutional lattice

sites, but the crystalline recovery of re-crystallized phase is insufficient. In other words, the annealing temperature higher than 1400°C is necessary for improving the mobilities, as well as for activating the impurities.

Figure 18 shows the IR reflectance spectra for the samples annealed for various annealing periods. The spectrum for the sample annealed for 0.5 min is almost the same as that for the sample annealed at 1400°C for 30 min. There is little change with annealing period up to 10 min in the reflectance spectra except for the oscillation periods. Since the oscillation periods are concerned with the thickness of the implanted layer, these changes suggest that the thickness of the implanted layers is changed by evaporation or precipitation in the implanted SiC layer. From the analysis, the thickness of the implanted layer d_{impla} decreases from 0.25 μm (0.5 min annealed) to 0.19 μm (10 min annealed), and the thickness of a graded-carrier-concentration layer increases from 0.05 μm to 0.08 μm . The volume fraction of defective SiC phase decreases drastically down to 2.9 % by 0.5 min annealing and is almost constant up to 10min. The derived annealing period dependence of free carrier concentration and mobility also shows that the recovering of the crystallinity and the electrical activation are sufficient by the annealing even for 0.5 min. These results indicate that the high temperature annealing as high as 1700°C puts the impurities onto substitutional lattice sites and recovers the crystallinity of the implanted layers within 1 min.

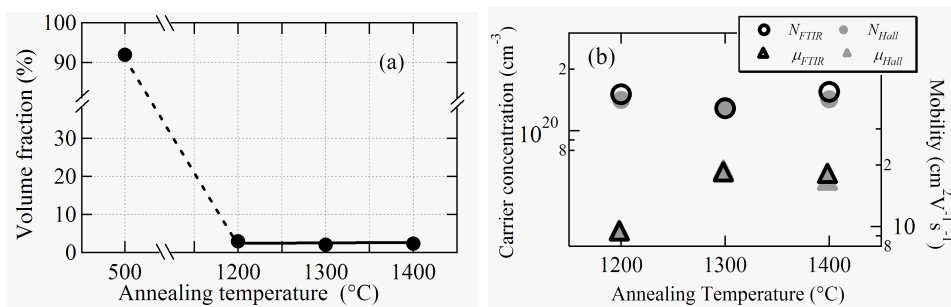


Figure 17. The annealing temperature dependences of (a) volume fraction of defective SiC phase, and (b) free carrier concentration and mobility in re-crystallized SiC phase. The values determined from Hall effect measurement also plotted in (b) for comparison [15].

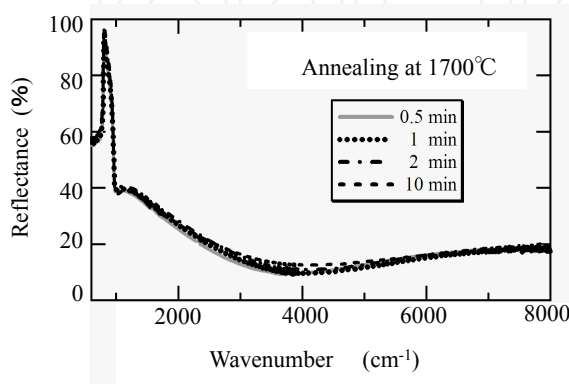


Figure 18. The IR reflectance spectra obtained from the samples annealed at 1700°C for various annealing periods [15].

5. Conclusion

We proposed the method for estimating the electrical properties, such as, carrier concentration and mobility of semiconductor wafers using IR reflectance spectroscopy. In the method, the observed spectra are fitted with the calculated ones, and the free carrier concentration and mobility are determined from the fitted parameters. In the calculation, we used the modified dielectric function (MDF) model for the dispersion relation of dielectric constants. We demonstrated the estimations of carrier concentrations and mobilities of commercially produced 6H-SiC wafers from observed IR reflectance spectra in the frequency range of 400–2000 cm^{-1} . We showed that the free carrier concentration and mobility obtained from IR reflectance measurements agree well with the values obtained from Hall-effect measurements in the carrier concentration range of $10^{17}\sim 10^{19}\text{ cm}^{-3}$, which suggests that we can estimate the carrier concentration and mobility accurately in a nondestructive and noncontact way. We demonstrated spatial mappings of carrier concentration and mobility in 2-inch 6H-SiC wafers using this method and showed its usefulness to characterize the spatial distribution of the carrier concentration and mobility in SiC wafers.

Next, we applied this method to the simultaneous determination of the carrier concentration, mobility and thickness of homo-epilayers, and the carrier concentration and mobility of substrates. IR reflectance spectra with the frequency range of 80–2000 cm^{-1} were measured for *n*-type 4H-SiC epilayers on *p*-type and *n*-type 4H-SiC substrates with different carrier concentrations. The obtained values of electrical properties for *n*-type epilayers on *p*-type substrates were compared with the values obtained from Hall-effect measurements, and those for *n*-type epilayers on *n*-type substrates were compared with the values from *C–V* measurements. Through these comparisons, we showed that the characterization method using IR reflectance measurements can determine the electrical property and the thickness of SiC homo-epilayers simultaneously and accurately. We also showed that the extension of the observation frequency range to Terahertz region (down to 20 cm^{-1}) enables us to characterize the wafers and epilayers with carrier concentrations ranged from 10^{16} to 10^{19}cm^{-3} orders.

Finally, we performed the characterization of both the electrical properties and crystalline damage in high-dose phosphorous implanted and post implantation annealed 4H-SiC layers using IR reflectance spectroscopy. The characterization revealed that the impurities are activated by annealing at a temperature as low as 1200°C for 30 min, though the sufficient recovery of the crystallinity needs higher annealing temperatures than 1200°C. It is also found from the IR reflectance analyses that the annealing at 1700°C activates the impurities and recovers the crystallinity of implanted layer within 1 min. These results suggest that the method can give the information of, not only the electrical properties, but also the crystalline damages of ion-implanted SiC epilayers simultaneously.

In conclusion, the electrical characteristics of SiC wafers and the electrical properties and thickness of SiC epilayers can be obtained simultaneously from the analyses of IR reflectance spectroscopy in nondestructive and contactless manner, which makes possible to obtain the spatial mapping of the electrical characteristics and thickness of SiC epilayers by scanning a probing light beam. Therefore, the method we proposed is a useful technique as

a monitoring tool of SiC device-process, i.e., the monitoring of the doping concentration, carrier mobility and thickness, and their uniformity over the wafers in homo-epitaxial growth process, and the recovery of crystallinity and electrical activation of impurities in post-implantation-annealing process.

Author details

Sadafumi Yoshida^{1*}, Yasuto Hijikata² and Hiroyuki Yaguchi²

*Address all correspondence to: s.yoshida@aist.go.jp

1 Advanced Power Electronics Research Center, National Institute of Advanced Industrial Science and Technology (AIST), Japan

2 Graduate School of Science and Engineering, Saitama University, Japan

References

- [1] Stibal, R., Muller, S., Jantz, W., Pozina, G., Magnusson, B., & Ellison, A. (2003). *Phys. Status Solidi*, C0, 1013.
- [2] Harima, H., Nakashima, S., & Uemura, T. (1995). Raman scattering from anisotropic LO-phonon-plasmon-coupled mode in n-type 4H- and 6H-SiC. *J. Appl. Phys.*, 78, 1996-2005.
- [3] Burton, J. C., Sun, L., Pophristic, M., Lukas, S. J., Long, F. H., Feng, Z. C., & Ferguson, I. T. (1998). Spatial characterization of doped SiC wafers by Raman spectroscopy. *J. Appl. Phys.*, 84, 6268-6273.
- [4] Chafai, M., Jaouhari, A., Terres, A., Anton, R., Martin, E., Jimenez, J., & Mitchel, W. C. (2001). Raman scattering from LO phonon-plasmon coupled modes and Hall-effect in n-type silicon carbide 4H-SiC. *J. Appl. Phys.*, 90, 5211-5215.
- [5] Yugami, H., Nakashima, S., Mitsuishi, A., Uemoto, A., Furukawa, K., Suzuki, A., & Nakashima, S. (1987). Characterization of the free-carrier concentrations in doped β -SiC crystals by Raman scattering. *J. Appl. Phys.*, 61, 354-358.
- [6] Tiwald, T. E., Woollam, J. A., Zoller, S., Christiansen, J., Gregory, R. B., Wetteroth, J. A., Wilson, S. R., & Powell, A. R. (1999). Carrier concentration and lattice absorption in bulk and epitaxial silicon carbide determined using infrared ellipometry. *Phys. Rev. B*, 60, 11464-11474.
- [7] Weingärtner, R., Wellmann, P. J., Bickermann, M., Hofman, D., Straubinger, T. L., & Winnacker, A. (2002). Determination of charge carrier concentration in n- and p-doped SiC based on optical absorption measurements. *Appl. Phys. Lett.*, 80, 70-72.

- [8] Holm, R. T., Gibson, J. W., & Palik, E. D. (1977). Infrared reflectance studies of bulk and epitaxial-film n-type GaAs. *J. Appl. Phys.*, 48, 212-223.
- [9] Holm, R. T., Klein, P. H., & Nordquist, P. E. R., Jr. (1986). Infrared reflectance evaluation of chemically vapor deposited β -SiC films grown on Si substrates. *J. Appl. Phys.*, 60, 1479-1485.
- [10] Macmillan, M. F., Henry, A., & Janzen, E. (1998). Thickness Determination of Low Doped SiC Epi-Films on Highly Doped SiC Substrates. *J. Electron. Mater.*, 27, 300-303.
- [11] Yaguchi, H., Narita, K., Hijikata, Y., Yoshida, S., Nakashima, S., & Oyanagi, N. (2002). Spatial Mapping of the Carrier Concentration and Mobility in SiC Wafers by Micro Fourier-Transform Infrared Spectroscopy. *Mater. Sci. Forum*, 389-393, 621-624.
- [12] Narita, K., Hijikata, Y., Yaguchi, H., Yoshida, S., & Nakashima, S. (2004). Characterization of Carrier Concentration and Mobility in n-type SiC Wafers Using Infrared Reflectance Spectroscopy. *Jpn. J. Appl. Phys.*, 43, 5156.
- [13] Oishi, S., Hijikata, Y., Yaguchi, H., & Yoshida, S. (2006). Simultaneous Determination of Carrier Concentration, Mobility, and Thickness of SiC homoepilayers by Infrared Reflectance Spectroscopy. *Jpn. J. Appl. Phys.*, 45, L1226-L1229.
- [14] Oishi, S., Hijikata, Y., Yaguchi, H., & Yoshida, S. (2007). Simultaneous Determination of the Carrier Concentration, Mobility and Thickness of SiC Homo-Epilayers Using Terahertz Reflectance Spectroscopy. *Mater. Sci. Forum*, 556-557, 423-426.
- [15] Narita, K., Hijikata, Y., Yaguchi, H., Yoshida, S., Senzaki, J., & Nakashima, S. (2004). Characterization of electrical properties in high-dose implanted and post-implantation-annealed 4H-SiC wafers using infrared reflectance spectroscopy. *Mater. Sci. Forum*, 457-460, 905-908.
- [16] Neyret, E., Ferro, G., Juillaguet, S., Bluet, J. M., Jaussaud, C., & Camassel, J. (1999). Optical investigation of residual doping species in 6H and 4H-SiC layers grown by chemical vapor deposition. *Materials Science and Engineering B*, 61-62, 253-257.
- [17] Nakashima, S., & Harima, H. (2004). Spectroscopic analysis of electrical properties in polar semiconductors with over-damped plasmons. *J. Appl. Phys.*, 95, 3541-3546.
- [18] Perkowitz, S. (1993). *Optical Characterization of Semiconductors*, Academic Press, London.
- [19] Perkowitz, S., & Thorland, R. T. (1975). Generalized Dielectric Function and the Plasmon-Phonon Coupling in GaAs and CdTe. *Solid State Commun.*, 16, 1093-1096.
- [20] Kukharskii, A. A. (1972). *Sov. Phys.-Solid State*, 14, 1501.
- [21] Pensl, G., & Choyke, W. J. (1993). Electrical and optical characterization of SiC. *Physica B*, 185, 264-283.
- [22] Chen, G. D., Lin, J. Y., & Jiang, H. X. (1975). Effects of electron mass anisotropy on Hall factors in 6H-SiC. *Appl. Phys. Lett.*, 68, 1341-1343.

- [23] Karmann, S., Suttrop, W., Schöner, A., Schadt, M., Haberstroh, C., Engelbrecht, F., Helbig, R., Pensl, G., Stein, R., & Leibenzeder, S. (1992). Chemical vapor deposition and characterization of undoped and nitrogen-doped single crystalline 6H-SiC. *J. Appl. Phys.*, 72, 5437-5442.
- [24] Iwata, H., & Itoh, K. M. (2001). Donor and acceptor concentration dependence of the electron Hall mobility and the Hall scattering factor in n-type 4H- and 6H-SiC. *J. Appl. Phys.*, 89, 6228-6234.
- [25] Iwata, H., Itoh, K. M., & Pensl, G. (2000). Theory of the anisotropy of the electron Hall mobility in n-type 4H- and 6H-SiC. *J. Appl. Phys.*, 88, 1956-1961.
- [26] Kinoshita, T., Itoh, K. M., Schadt, M., & Pensl, G. (1999). Theory of the electron mobility in n-type 6H-SiC. *J. Appl. Phys.*, 85, 8193-8198.
- [27] Volm, D., Meyer, B. K., Hofman, D. M., Chen, W. M., Son, N. T., Persson, C., Lindefelt, U., Kordina, O., Sorman, E., Konstantinov, A. O., Monemar, B., & Janzen, E. (1996). Determination of the electron effective-mass tensor in 4H SiC. *Phys. Rev. B*, 53, 15409-15412.
- [28] Kojima, K., Suzuki, T., Kuroda, S., Nishio, J., & Arai, K. (2003). Epitaxial Growth of High-Quality 4H-SiC Carbon-Face by Low-Pressure Hot-Wall Chemical Vapor Deposition. *Jpn. J. Appl. Phys.*, 42, L637-L639.
- [29] Rutsch, G., Devaty, R. P., Choyke, W. J., Langer, D. W., & Rowland, L. B. (1998). Measurement of the Hall scattering factor in 4H and 6H SiC epilayers from 40 to 290 K and in magnetic fields up to 9 T. *J. Appl. Phys.*, 84, 2062-2064.
- [30] Götz, W., Schöner, A., Pensl, G., Suttrop, W., Choyke, W. J., Stein, R., & Leibenzeder, S. (1993). Nitrogen donors in 4H-silicon carbide. *J. Appl. Phys.*, 73, 3332-3338.
- [31] Capano, M. A., Cooper, J. A., Jr., Melloch, M. R., Saxler, A., & Mitchel, W. C. (2000). Ionization energies and electron mobilities in phosphorus- and nitrogen-implanted 4H-silicon carbide. *J. Appl. Phys.*, 87, 8773-8777.
- [32] Nishio, J., Kushibe, M., Masahara, K., Kojima, K., Oono, T., Ishida, Y., Takahashi, T., Suzuki, T., Tanaka, T., Yoshida, S., & Arai, K. (2002). Investigation of Residual Impurities in 4H-SiC Epitaxial Layers Grown by Hot-Wall Chemical Vapor Deposition. *Mater. Sci. Forum*, 389-393, 215-218.
- [33] Chang, W. Z., Feng, Z. C., Lin, J., Liu, R., Wee, A. T. S., Tone, L., & Zhao, J. H. (2002). Infrared reflection investigation of ion-implanted and post-implantation-annealed epitaxially grown 6H-SiC. *Surf. Interface Anal.*, 33, 500-505.
- [34] Camassel, J., Wang, H. Y., Pernot, J., Godignon, P., Mestres, N., & Pascual, J. (2002). Infrared Investigation of Implantation Damage in 6H-SiC. *Mater. Sci. Forum*, 389-393, 859-862.
- [35] Senzaki, J., Fukuda, K., & Arai, K. (2003). Influences of postimplantation annealing conditions on resistance lowering in high-phosphorus-implanted 4H-SiC. *J. Appl. Phys.*, 94, 2942-2947.